

Three-Body Binary Formation in Clusters: Analytical Theory

Yonadav Barry Ginat,^{1,2*} and Hagai B. Perets³

¹*Rudolf Peierls Centre for Theoretical Physics, University of Oxford, Parks Road, Oxford, OX1 3PU, United Kingdom*

²*New College, Holywell Street, Oxford, OX1 3BN, United Kingdom*

³*Faculty of Physics, Technion – Israel Institute of Technology, Haifa, 3200003, Israel*

Accepted XXX. Received YYY; in original form ZZZ

ABSTRACT

Binary formation in clusters through triple encounters between three unbound stars, ‘three-body’ binary formation, is one of the main dynamical formation processes of binary systems in dense environments. In this paper, we use an analytical probabilistic approach to study the process for the equal mass case and calculate a probability distribution for the orbital parameters of three-body-formed binaries, as well as their formation rate. For the first time, we give closed-form analytical expressions to the full orbital parameter distribution, accounting for both energy and angular momentum conservation. This calculation relies on the sensitive dependence of the outcomes of three-body scatterings on the initial conditions: here we compute the rate of three-body binaries from ergodic interactions, which allow for an analytical derivation of the distribution of orbital parameters of the binaries thus created. We find that soft binaries are highly favoured in this process and that these binaries have a super-thermal eccentricity distribution, while the few hard three-body binaries have an eccentricity distribution much closer to thermal. The analytical results predict and reproduce simulation results of three-body scattering experiments in the literature well.

Key words: galaxies: clusters: general – chaos – (stars:) binaries: general – stars: kinematics and dynamics

1 INTRODUCTION

Binary stars are among the most important astrophysical systems, playing a key part in stellar evolution, and in the dynamics of dense stellar systems. They have a major role in the evolution of globular clusters (e.g. [Heggie & Hut 2003](#); [Binney & Tremaine 2008](#)), and effectively serve to stop core-collapse (e.g. [Hut 1996](#); [Goodman & Hut 1989](#)). Among the leading channels for the formation of binaries in clusters are primordial binaries formed in the first epoch of star formation in the cluster (e.g. [Shu et al. 1987](#)), tidal captures (e.g. [Fabian et al. 1975](#); [Press & Teukolsky 1977](#); [Generozov et al. 2018](#)), and dynamical formation of binaries, via three-body interaction – so-called ‘three-body’ binaries (e.g. [Mansbach 1970](#); [Aarseth & Heggie 1976](#); [Stodolkiewicz 1986](#); [Goodman & Hut 1993](#); [Portegies Zwart & McMillan 2000](#); [Heggie & Hut 2003](#); [Atallah et al. 2024](#)), which are the topic of this paper – see, e.g. [Pooley et al. \(2003\)](#) for observational evidence for this process. In such an interaction, three unbound bodies exchange energy, such that at the end two of them remain bound, with the third one serving as a cata-

lyst, an energy reservoir where excess energy is deposited. Incidentally, it has been proposed recently that if sufficient amounts of gas are present in a cluster, this could accelerate binary formation by serving as a dissipation mechanism – an alternative energy reservoir ([Rozner et al. 2023](#)).

In this paper, we wish to study three-body binary formation from an analytical perspective. We seek to offer a complimentary calculation to those of [Aarseth & Heggie \(1976\)](#), who approached the problem in an impulsive approximation, and [Goodman & Hut \(1993\)](#), who used detailed balance to convert an analysis of the inverse problem – that of the ionisation of a binary by a single star, to three-body binary formation. Here, instead, we would like to harness the chaotic nature of the three-body problem (e.g. [Valtonen & Karttunen 2006](#)) to derive probabilistic results on three-body binary formation. While previous analytical works on the probabilistic solution of the three-body problem (e.g. [Monaghan 1976a,b](#); [Valtonen & Karttunen 2006](#); [Stone & Leigh 2019](#); [Ginat & Perets 2021a,b](#); [Kol 2021](#)) have studied the negative energy case, i.e. a binary-single encounter, here we study the positive-energy case – the formation of a binary from three initially unbound stars. This approach allows us to calculate not only the binary formation rate but also the

* E-mail: yb.ginat@physics.ox.ac.uk

joint eccentricity and semi-major axis distribution, in a way that accounts for angular momentum conservation as well as energy conservation, during the three-body interaction.

The three-body binary formation can be automatically accounted for in N -body simulations of globular clusters, if close encounters are well resolved, and not smeared by artificial softening (e.g. van Albada 1968; Aarseth 1969; Breen & Heggie 2012a,b; Tanikawa 2013; Wang et al. 2016; Park et al. 2017; Kumamoto et al. 2019; Arca Sedda et al. 2023), but not necessarily in Monte-Carlo simulations (e.g. Giersz 1998; Ivanova et al. 2005; Morscher et al. 2015; Geller et al. 2019; Hong et al. 2020; Rodriguez et al. 2022; Weatherford et al. 2023), which often resort to implementing a prescription for three-body binary formation (Ivanova et al. 2005). The former simulations are often limited, as modelling realistic globular clusters, requires expensive long-term simulations, as such clusters are old, highly populated, and diverse – and thus too computationally expensive – to be accurately modelled by direct N -body simulations. Moreover, few-body simulations do not provide an inherent understanding of the formation process and its dependence on the properties of the encounters. It is thus important to derive an analytic understanding of the processes. Moreover, such analysis can test and replace semi-analytic prescriptions used in Monte-Carlo simulations, which are more versatile than direct N -body ones.

The paper is structured as follows: we start by calculating the probability distribution of binary parameters, *given* fixed values of the conserved quantities – the energy and angular momentum (as well as the masses) in §2. This allows us to study the properties of binaries formed this way as a function of these parameters. Then, in §3, we consider the binary formation rate in a system, e.g. a globular cluster, given a distribution of initial positions and velocities. In both sections, we endeavour to keep the lengthier calculations to appendices, while quoting the physical results in the main text. In §5 we summarise the results and highlight their implications. In this paper, we consider strictly the equal mass case, although many of the formulae derived here extend immediately to the unequal case (in particular, most of §2).

In the final stages of this work, Atallah et al. (2024) published a *numerical* study of the three-body binary formation. They analysed the results of three-body numerical experiments with positive energy, which provides us with direct data to test our analytic predictions. We therefore structured the calculation of the binary-formation rate in §3 to allow for a simple comparison with their results. As the results of Atallah et al. (2024) are integrated over a distribution of energies and angular momenta, the calculations of §2 are not immediately comparable with them, (but as tested via their integrals in §3).

2 RESONANT UNBOUND THREE-BODY SCATTERINGS

Consider three bodies coming from infinity, with masses m_1 , m_2 , and m_3 , and total energy $E > 0$ and angular momentum \mathbf{J} . For point particles, the possible scattering outcomes are: (i) three unbound stars, or (ii) a bound binary and a single unbound star. In this section, we focus on the probability for

the outcome (ii), for a given set of conserved quantities, i.e. for given values of E , and the total angular momentum (in the centre-of-mass frame), \mathbf{J} . To do so, we have to describe the allowed region of phase-space (in §§2.1 and 2.2). The resultant orbital parameter distribution follows, from which we derive scaling relations with the spatial cut-off (see below) and the hard-soft-boundary.

The phase-space volume for a positive-energy three-body system is infinite, so we must require that the three bodies interact inside a region of size R_0 , which will be described in §2.1 below. For now, suffice it to say that if they don't, then for $R_0 \rightarrow \infty$, the interaction is not chaotic, so indeed these should be excluded.

If the outcome is a bound binary and a single star, then we label the remnant binary parameters with a sub-script b , and those of the orbit of the single star about the binary's centre of mass with a sub-script s . However, we still do that if there are three unbound stars, simply reserving the sub-script b for the pair with the lowest two-body energy, and we still refer to this pair as a 'binary', albeit unbound.

Then, in principle, as long as the outcome is highly sensitive to initial conditions, one can still apply the theory of approximate solutions to the three-body problem, similar to situations with negative total energy. While there are no prolonged democratic resonances – phases during which the particles are in approximate energy equipartition (Heggie & Hut 1993) – in a positive-energy three-body interaction, we contend that the question of binary formation still depends very sensitively on the initial conditions, because the energy exchanges required to form binaries are as large as the total energy, and the general three-body problem is chaotic. Therefore, while one, single scattering problem does not cover all the available phase space, an ensemble of them would, which is the more relevant case for astrophysical applications. The results of this paper can be viewed as a calculation of the distribution of the ergodic subset of three-body binary formation.

Under these assumptions, we find (Ginat & Perets 2021a) that the outcome probability distribution $f(E_b, \mathbf{S}|E, \mathbf{J})$ for the binary's orbital parameters (those of the outer orbit are automatically given by conservation laws) is

$$f(E_b, \mathbf{S}|E, \mathbf{J}) \propto m_b \frac{\theta_{\max}(R_0, E_b, S) \theta_{\max}(R_s, E_s, |\mathbf{J} - \mathbf{S}|)}{|\mathbf{J} - \mathbf{S}| E_s^{3/2} |E_b|^{3/2}}, \quad (1)$$

where $E_s = E - E_b$, *etc.*, and θ_{\max} is a function of its arguments, explicitly defined in Stone & Leigh (2019, supplementary information; denoted l_{\max} there). The quantity R_s will be defined in §2.2 below. The second factor of θ_{\max} is the usual one (Stone & Leigh 2019), which comes from integrating over the mean anomaly of the outer orbit, explicitly accounting for the finite distance the ejected star can have from the centre of mass of the binary as the triple leaves the strong-interaction region. The first factor of θ_{\max} has a similar origin: if $E_b > 0$, the mean anomaly of the binary is also likewise restricted, by R_0 : essentially, we require that the separation of the binary be smaller than R_0 . As $\theta_{\max}(R, E, L) \sim R^{-3/2} E^{3/2}$, the first factor of θ_{\max} cancels the divergence at $E_b = 0$, while the second one cancels the divergence of $E_s^{-3/2}$ at $E_s = 0$. The parameter R_s is defined

as in equation (10) of [Ginat & Perets \(2021a\)](#) for the $E < 0$ case, and in §2.2 below for $E > 0$.

2.1 Cut-Offs

The only thing left to specify is the dependence of R_0 on the conserved quantities. We envisage two possibilities for R_0 : first, one may approximate R_0 by the ‘virial’ radius

$$R_0 \approx R_E \equiv \frac{G(m_1m_2 + m_1m_3 + m_2m_3)}{6E} = \frac{GM_2^2}{2E}, \quad (2)$$

where we have defined

$$M_2 \equiv \sqrt{\frac{m_1m_2 + m_2m_3 + m_1m_3}{3}}. \quad (3)$$

This captures the intuition, that the distance of the closest approach of the triple should be such that the potential energy is of the same order of magnitude as the kinetic energy, at least there. Otherwise, a large energy exchange – necessary for the formation of hard binaries – is unlikely. Alternatively, the other possibility is to relax this requirement, and simply demand that the distance of the closest triple approach be less than the system’s Hill radius, i.e. that at least there, the interaction is a three-body interaction (to leading order), and that the other cluster stars can be neglected. This amounts to

$$R_0 \approx d, \quad (4)$$

where $d \equiv n^{-1/3}$, with n being the cluster’s number density. As mentioned above, d may be defined as the binary’s Hill radius in its motion in the cluster, by equating the tidal force that the latter exerts on it with its own gravity, in which case $d \propto M^{1/3}$. For our purposes, what matters is that d is independent of the triple’s energy or angular momentum. The possible definitions are

$$R_0 = \begin{cases} \min\{R_E, d\} & \text{case 1;} \\ d & \text{case 2.} \end{cases} \quad (5)$$

While case 2 might be more justifiable as more generic, the first, more restrictive case is required for significant energy exchanges, if a hard binary is to be produced. We will discuss both choices for R_0 in this paper.

2.2 Additional Phase-Space Constraints

Contrary to the negative-energy three-body problem, it is strictly impossible for a positive-energy triple to exist in a democratic resonance for an extended time. This implies that there could be triple configurations that cannot dynamically arrive at a binary-single system, despite having the right conserved quantities. Hence, one must impose additional constraints, to ensure that a triple encounter would be able to form a binary. The fundamental assumption of this work is that after these extra ones are imposed, the system *is* able to reach all the allowed binary-single configurations. Though the above-mentioned various assumptions are not trivial, the successful comparison with the few-body results supports their validity.

While for the negative energy three-body problem, in the case that a hard binary forms, the single star can be

ejected at a distance $r_s \leq R_-$ from the centre of mass of the remnant binary, with ([Ginat & Perets 2021a](#))

$$R_- = \beta \min \left\{ a_b, \left(\frac{G\mu_b\mu M}{m_b|E|} \right)^{1/3} a_b^{2/3} \right\}, \quad (6)$$

where we use $\beta = 1.5$ as in [Ginat & Perets \(2023\)](#). However, in our case, there are two complications: (i) the remnant binary might not be hard, i.e. it might have $a_b \gg \frac{G\mu_b\mu M}{m_b|E|}$, and (ii) it could be unbound completely.

For case (ii), there is no binary formation, which means that there is no restriction on the ejection of star s at all, and in that case, $r_s \leq R_0$ is the only condition. Besides, for marginally bound binaries (case (ii)), the requirement $r_s \leq R_-$ does not make sense any more, because it stemmed from a requirement of a hierarchy of energies ([Ginat & Perets 2021a](#)), which becomes invalid. Instead, we extend the unbound upper limit to these binaries. For $0 < \varepsilon \ll 1$, if $|E_b| < \varepsilon Gm_b\mu_b/(2R_0)$, we therefore also only require $r_s \leq R_0$. We choose $\varepsilon = 1/10$, but have verified that the results remain unchanged up to $\varepsilon = 1/100$.

In summary, the cut-off on the separation r_s between the single star and the centre-of-mass of the other two, when the interaction is deemed to have terminated, is $r_s \leq R_s$, where

$$R_s = \begin{cases} \min\{R_-, R_0\} & \text{if } E_b < -\varepsilon \frac{Gm_b\mu_b}{2R_0} \\ R_0 & \text{otherwise.} \end{cases} \quad (7)$$

It is this R_s that enters the θ_{\max} in equation (1).

2.3 Binary Formation For Fixed Conserved Quantities

When evaluated using techniques similar to those of [Ginat & Perets \(2021a\)](#), the marginal energy distribution of the remnant binary we find is shown in figure 1.

As only the second θ_{\max} depends on the inclination, one can derive a marginal eccentricity-energy distribution, given that a bound binary forms, in much the same manner as [Ginat & Perets \(2023\)](#). The result is

$$f_{\text{bd}}(E_b, S|E, \mathbf{J}) \propto m_b \frac{\theta_{\max}(R_0, E_b, S)\theta_{\text{ap}}(R_s, E_s)}{E_s^{3/2}|E_b|^{3/2}} \frac{A_p \Delta\psi}{J}, \quad (8)$$

where $\Delta\psi$ and A_p are defined in that work (equation (4) there and the text around it). The marginal eccentricity distribution is plotted in figure 2. Due to the extra factor of $\theta_{\max}(R_0, E_b, S)$, the result is highly non-thermal, even for large values of the total angular momentum J . Intuitively, the reason that this distribution is super-thermal, is because of the additional factor of $\theta_{\max}(R_0, E_b, S)$: this introduces a constraint on the pericentre – namely that it be smaller than R_0 , which is of course easier to fulfil when the eccentricity is high; thus, there is more phase-space volume associated with high eccentricity that the binary can occupy. The joint energy-eccentricity distribution is plotted in figure 3, for different values of the parameter

$$\kappa \equiv \frac{J^2|E|}{G^2M^2\mu^3}. \quad (9)$$

One can see immediately that the softest binaries – those

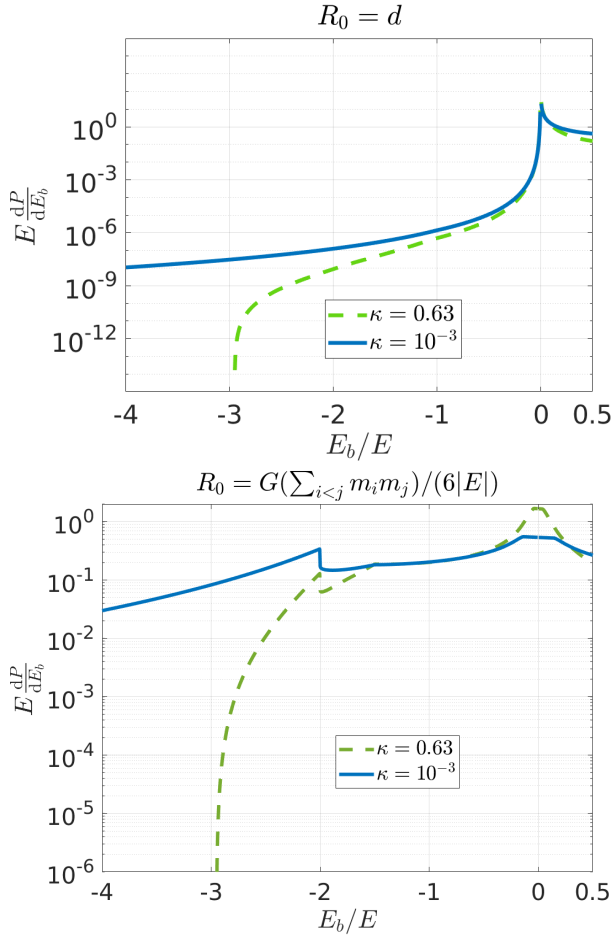


Figure 1. The marginal energy distribution of the remnant binary, for equal masses. Top: $R_0 = d$, with $d = 150GM\mu/E$. Bottom: the case $R_0 = \min\{R_E, d\}$.

with large $E/|E_b|$ – tend to be the most eccentric. If the system is in a cluster with temperature T , another dimensionless parameter we will require is ζ , defined by

$$\zeta \equiv \frac{GM^2}{R_0 k_B T}. \quad (10)$$

The total probability that a binary form is just the integrand of equation (1) over $E_b < 0$. This is plotted in figure 4, as a function of the only non-dimensional combination of conserved quantities available, for equal masses, i.e. of κ , for both options for R_0 considered here, for a fixed d . One can see that when J becomes too large, the probability of hard binary formation plummets to 0.

An inspection of figure 4 shows that p_{bin} changes very little with κ , from 0.1257 to 0.2353 in the range plotted. This is true, of course, only for low values of κ , because κ is bounded from above by Sundman’s inequality (Sundman 1913), which effectively implies that there exists an upper bound κ_{max} above which $p_{\text{bin}} = 0$. We give explicit expressions for κ_{max} in appendix A. When evaluating the rate in §3 below, we therefore approximate it as a constant, *viz.*

$$p_{\text{bin}}(\kappa) \approx \bar{p}_{\text{bin}} \Theta(\kappa_{\text{max}} - \kappa), \quad (11)$$

with \bar{p}_{bin} being the mean value of $p_{\text{bin}}(\kappa)$, and Θ is Heavi-

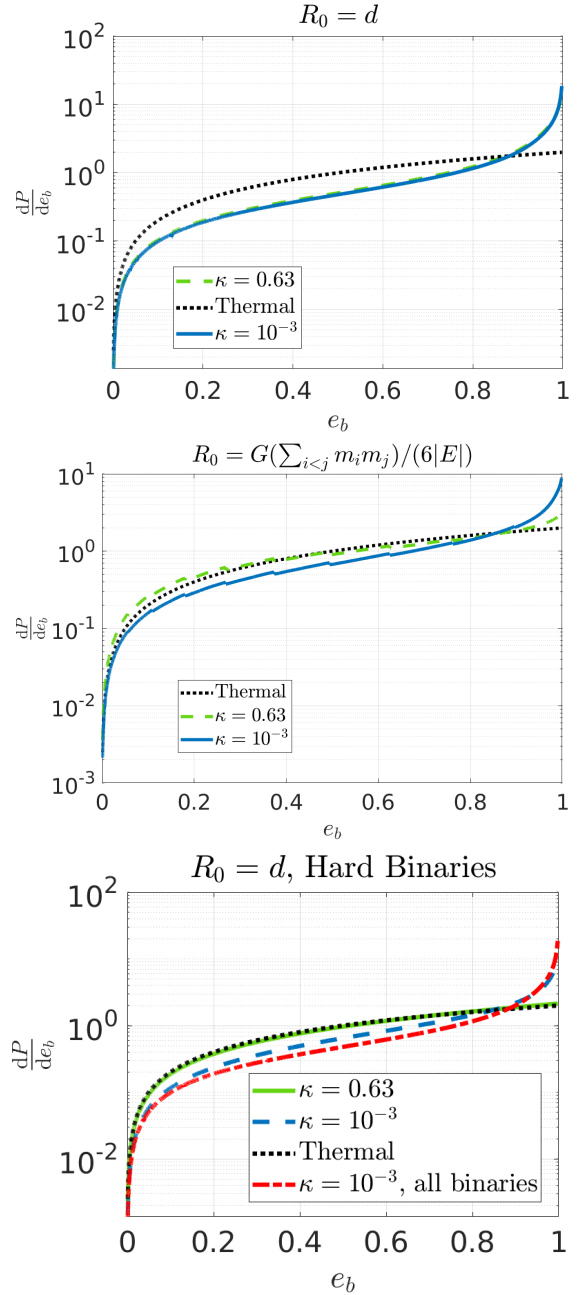


Figure 2. The marginal eccentricity distribution of the remnant binary, given that the remnant binary is bound, for equal masses. This is calculated by integrating equation (8) over the domain $E_b < 0$ (and normalising). Top: $R_0 = d$, with $d = 150GM\mu/E$; middle: the case $R_0 = \min\{R_E, d\}$; bottom: same as the top panel, but for hard binaries only, i.e. those with $|E_b| \geq E$.

side’s function. \bar{p}_{bin} still depends on R_0 , as will be explained below. It is 0.1574 for $R_0 = 150GM\mu/E$ in the top panel of figure 4.

2.4 Hard-Binary Formation

The probability of the formation of a hard binary is

$$p_{\text{hard}} = \int_{-\infty}^{-k_B T} dE_b \int dS f_{\text{bd}}(E_b, S|E, \mathbf{J}). \quad (12)$$

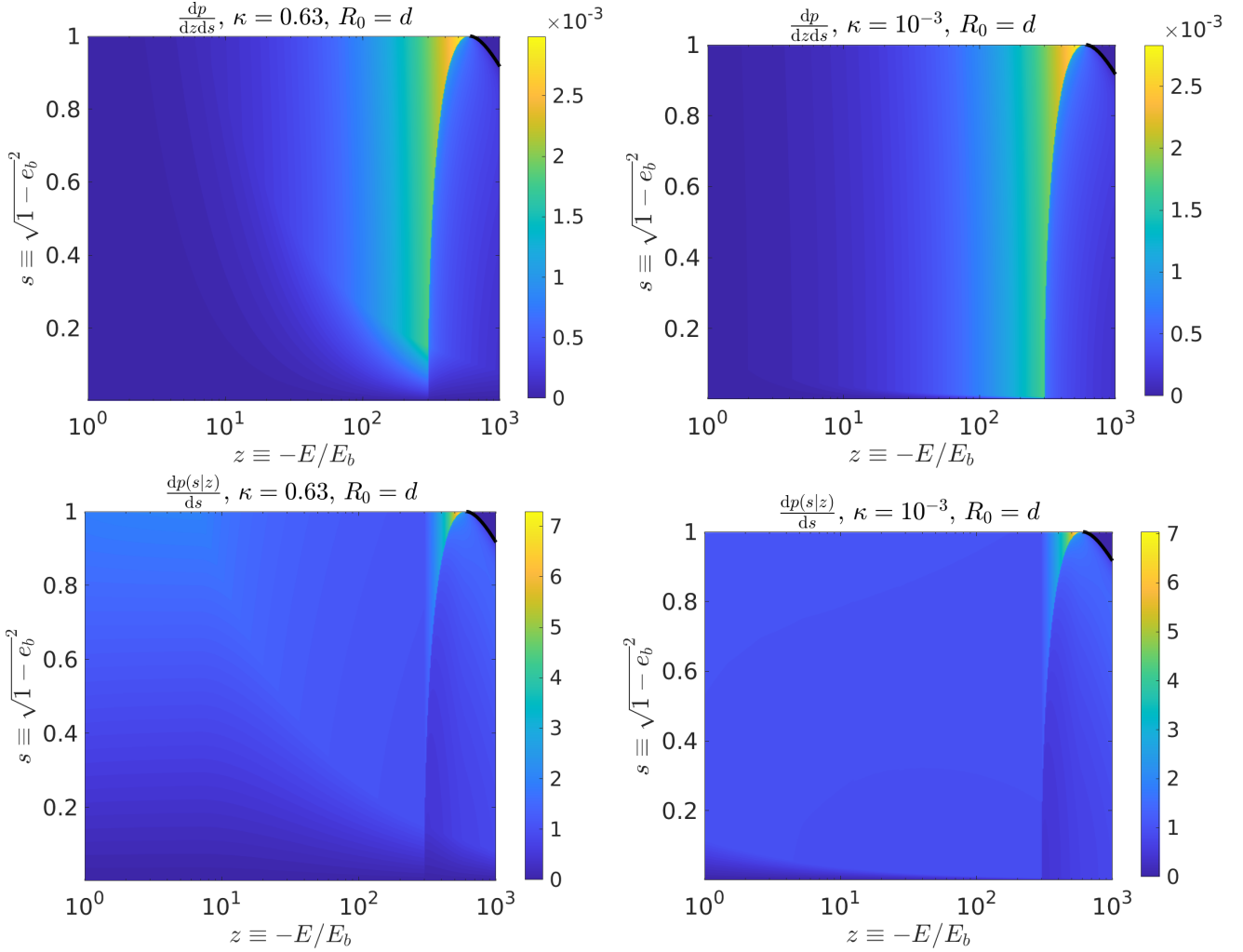


Figure 3. The joint energy-eccentricity distribution of the remnant binary, i.e. equation (8), given that the remnant binary is bound, for equal masses. The plots in the top row show the distribution for different values of the parameter $\kappa = \frac{J^2|E|}{G^2M^2\mu^3}$. The plots in the bottom row are the probability distributions for the dimensionless angular momentum $s \equiv \sqrt{1 - e_b^2}$, given z . The black line is the line $e_b = 1 - R_0/a_b$ – values of s above that threshold cannot form.

This is closely related to the quantity

$$p_0 \equiv \int_{-\infty}^{-E} dE_b \int dS f_{\text{bd}}(E_b, S|E, \mathbf{J}). \quad (13)$$

For a fixed value of $R_0 = d_0$, p_0 depends only on κ , but f_{bd} scales like (energy) $^{-3}$, so its integral scales like (energy) $^{-2}$; additionally, $\kappa \propto E$, and therefore

$$p_{\text{hard}} = \left[\frac{E}{k_{\text{BT}}} \right]^2 p_0 \left(\kappa \frac{k_{\text{BT}}}{E} \right). \quad (14)$$

We test this scaling in appendix B, where we also explain why

$$p_{\text{bin}} \propto R_0^{-1/2} \quad (15)$$

$$p_{\text{hard}} \propto \frac{G^2 M^4}{R_0^2 E^2}$$

in the limit where $\frac{GM^2}{R_0 E} \ll 1$. (Let us stress that this is not true for $\frac{GM^2}{R_0 E}$ of order unity.) This, and the above, imply

that the entire dependence of p_{hard} on the parameters at hand is

$$p_{\text{hard}} = \left[\frac{E}{k_{\text{hBT}}} \right]^2 \left[\frac{d_0}{R_0} \right]^2 p_0 \left(\kappa \frac{k_{\text{BT}}}{E}; R_0 = d_0 \right). \quad (16)$$

This scaling behaviour allows us to calculate p_{hard} for one set of values of the parameters R_0 and k_{BT} , tabulate it and use that when computing the hard binary formation probability at any value of the parameters, and any κ . This will simplify the rate calculation in the next section considerably.

3 BINARY FORMATION RATE CALCULATION

So far, we have explored the binary formation probability for fixed total energy and angular momentum. In a realistic cluster, of course, these vary from one interaction to another, and a more relevant quantity is the average value of p_{bin} , over an ensemble of triples, with a certain distribution of

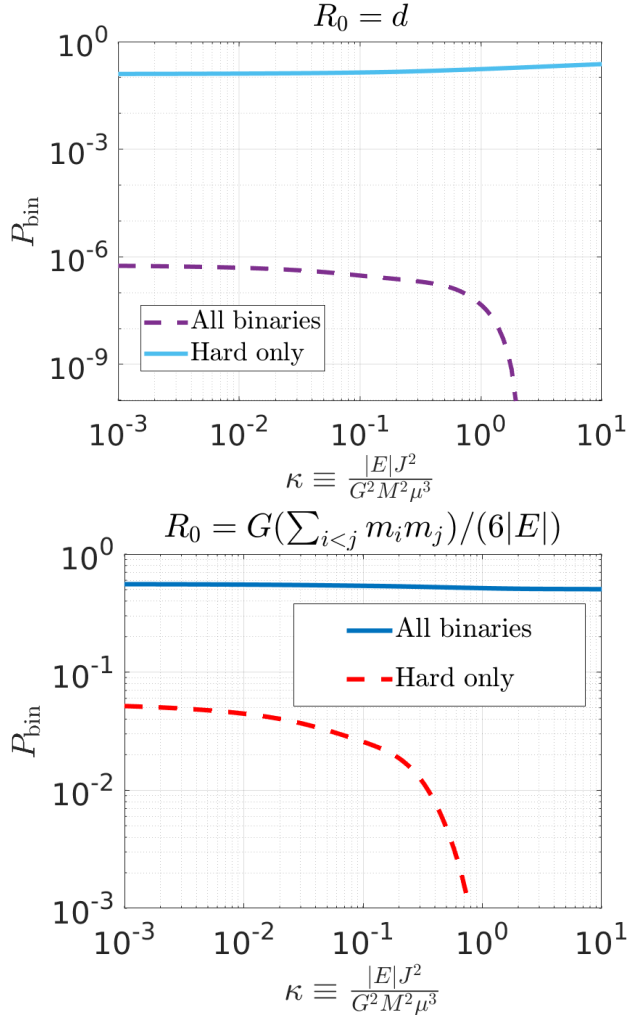


Figure 4. The binary formation probability, as a function of the angular momentum, made dimensionless, for equal masses. *Top:* the case $R_0 = d$, with $d = 150 GM\mu/E$; *bottom:* the case $R_0 = R_E$. As hard binaries require significant energy exchanges to form, essentially all hard binaries form for $R_0 \leq R_E$, so that their relative fraction is lower when R_0 can be larger – because only soft binaries form at $R_E \leq R_0 \leq d$.

initial conditions. The purpose of this section is to find this probability, which we call P_{bin} , and to characterise it.

The rate calculation follows [Aarseth & Heggie \(1976\)](#) (see also [Goodman & Hut 1993](#); [Ivanova et al. 2005](#)). The rate per star, at which a star of m_1 becomes (on average) involved in a 3-body interaction leading to the formation of a binary with component masses m_1 and m_2 , is given by

$$\Gamma = \frac{n_2 n_3 (m_1 m_2 m_3)^{3/2}}{(2\pi k_B T)^3 M^{3/2}} \int d^3 v \int d^3 V \int dr \int dR \quad (17)$$

$$2\pi r v 4\pi R^2 e^{-\frac{\mu_b v^2}{2k_B T} - \frac{\mu V^2}{2k_B T}} p_{\text{bin}}.$$

The integration domain for R and r depends on the initial condition distribution. Here, all stars are assumed to have a Gaussian velocity distribution with temperature T , and the triple’s centre-of-mass motion has already been integrated

out. The Jacobi coordinates are

$$\mathbf{R} \equiv \mathbf{x}_3 - \frac{m_1 \mathbf{x}_1 + m_2 \mathbf{x}_2}{m_b} \quad (18)$$

$$\mathbf{r} \equiv \mathbf{x}_2 - \mathbf{x}_1, \quad (19)$$

and \mathbf{V} and \mathbf{v} are their respective associated velocities, where \mathbf{x}_n is the position of star n .

The rate per unit volume (instead of per star) is simply equation (17) multiplied by n_1 , i.e.

$$\Gamma_v = \frac{n_1 n_2 n_3 (m_1 m_2 m_3)^{3/2}}{(2\pi k_B T)^3 M^{3/2}} \int d^3 v \int d^3 V \int dr \int dR \quad (20)$$

$$2\pi r v 4\pi R^2 e^{-\frac{\mu_b v^2}{2k_B T} - \frac{\mu V^2}{2k_B T}} p_{\text{bin}}.$$

By the law of total probability, Γ_v factories into a product of the total interaction rate, Γ_{3UB} , and the probability that a binary forms, given a three-body interaction, P_{bin} . The former evaluates to ([Atallah et al. 2024](#))

$$\Gamma_{\text{3UB}} = \frac{8\pi^{3/2}}{3\sqrt{2}} R_0^5 n_1 n_2 n_3 \sigma, \quad (21)$$

where it is assumed that the bodies have random positions, uniformly distributed in a sphere of radius R_0 , and a Gaussian velocity distribution, with a 1-dimensional dispersion σ .

Then, $\Gamma_v = \Gamma_{\text{3UB}} P_{\text{bin}}$, where

$$P_{\text{bin}} = \frac{1}{V_0^2} \left(\frac{m_1 m_2 m_3}{M} \right)^{3/2} \frac{1}{(2\pi k_B T)^3} \int d^3 r d^3 R d^3 v d^3 V \quad (22)$$

$$e^{-\frac{E}{k_B T}} p_{\text{bin}}(\kappa(E, J); R_0).$$

As mentioned above, the binary formation probability, p_{bin} , given a triple interaction, is only a function of κ and R_0 in the equal-mass case, but may also depend on the mass-ratios if they are unequal. At any rate, we calculate it directly by integrating equation (1) over the allowed parameter space (for a bound remnant binary), summing over the three possibilities for star s , and normalising.

A perhaps more interesting quantity is obtained by replacing p_{bin} by the probability for creating a *hard* binary, p_{hard} , which gives the rate of formation of hard 3-body binaries, which we denote by P_{hard} . The non-trivial shape of $p_{\text{hard}}(\kappa)$ (see figure 4) requires a more complicated calculation; both calculations, for P_{hard} and P_{bin} are performed in appendix C. We restrict the calculations to the $\zeta \ll 1$ régime, which is the physically relevant one. We now move on to describe the integration domain and derive P_{bin} , P_{hard} , the rate, and the orbital parameter distribution.

3.1 Occurrence of an Interaction

As alluded to above in §2, for a binary to form, one of the stars must pass sufficiently close to the centre of mass of the other two, to exchange enough energy with them to make them bound. This is not encapsulated in the κ dependence of p_{bin} *per se* and must be imposed explicitly when evaluating the integrals for P_{bin} and P_{hard} because while the outcome does depend sensitively on the initial conditions, it does not only depend on them via κ .

We can derive a necessary condition for this to happen, based on the minimum requirement of a strong enough

perturbation in the impulsive limit (cf. [Aarseth & Heggie 1976](#)). In the time-reversed configuration, where a single star ionises a binary, it is required, at a minimum, that the star would be able to give the binary enough energy to unbind it. That is, in the impulse approximation (which is a lower limit)

$$\sqrt{\frac{Gm_b}{a_b}} \frac{2Gm_s}{r_s V} \geq \frac{Gm_b}{2a_b}; \quad (23)$$

this should be multiplied by $\sqrt{2}$ because both stars are affected. Hence,

$$r_s \leq 4\sqrt{\frac{Gm_s^2 \mu_s a_b}{E_s m_b}}. \quad (24)$$

We therefore restrict R as follows: firstly, $R \leq R_0$, and additionally,

$$R \leq \begin{cases} \sqrt{8 \frac{G^2 m_s^2 \mu_s \mu_b}{E_s^i E_b^i}} & \text{hard only} \\ \frac{2Gm_s}{V} \sqrt{\frac{r}{2Gm_b}} & \text{all binaries,} \end{cases} \quad (25)$$

where here $E_s^i = \mu_s V^2/2$ and $E_b^i = \mu_b v^2/2$. The first case is the same as (24); the second case is less stringent because, for the formation of a soft binary, we require merely that one of the stars impart an impulse on the other two, which is as large as their relative momentum at (hyperbolic) pericentre. Whether subsequent interactions in the same encounter then form a binary is determined by p_{bin} .

3.2 Computation of The Formation Probability

We are now in a position to evaluate the integrals in equation (22), both for P_{bin} and for the analogous P_{hard} . This is done in appendix C, where we also show analytically that, as functions of ζ ,

$$P_{\text{bin}} \sim P_{\text{bin}}(\zeta_0) \left(\frac{\zeta}{\zeta_0}\right)^2 \propto \chi_1^{-2}, \quad (26)$$

$$P_{\text{hard}} \sim P_{\text{hard}}(\zeta_0) \left(\frac{\zeta}{\zeta_0}\right)^5 \propto \chi_1^{-5},$$

as $\zeta \rightarrow 0$. In particular, this implies that as $R_0 \rightarrow \infty$, both Γ and Γ_v tend to a constant, for hard binaries, but grow as R_0^3 if one wishes to include soft binaries, too.

We show the full results of calculating P_{bin} and P_{hard} as functions of ζ , for the equal mass case in figure 5. We plot them as functions of a dimension-less parameter $\chi_1 \propto 1/\zeta$, which is defined in [Atallah et al. \(2024\)](#), for ease of comparison. In the equal mass case, $\chi_1 = 27/(2\zeta)$. We see good agreement between our results and those of [Atallah et al. \(2024\)](#).¹ Surprisingly, the asymptotic χ_1 dependence is not reached until very large values of χ_1 . The two curves, $P_{\text{hard},1}$ and $P_{\text{hard},2}$ are plotted when using the first of conditions (25) or the second for hard binaries, respectively (equations (C14) and (C18)).

It is also instructive to compare the total hard binary

¹ The procedure whereby the initial conditions are changed in that work, as the particles are moved backward along their initial velocity vectors, changes neither the angular momenta nor, in the limit $\zeta \ll 1$, the energies, so we disregard it here.

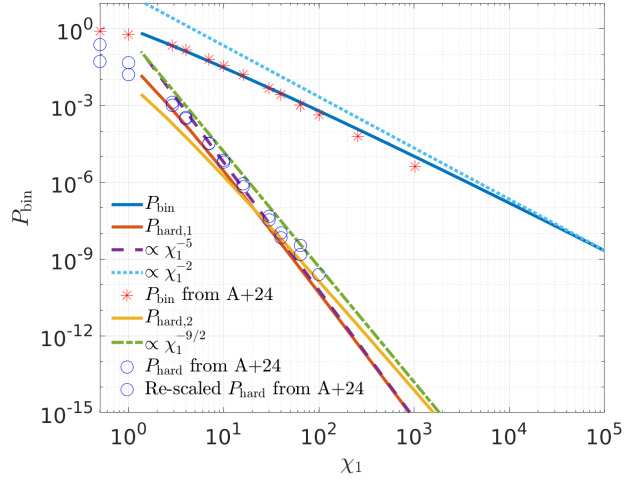


Figure 5. The binary formation probability, as a function of $\chi_1 = 27/(2\zeta)$, for equal masses. This assumes a density $n = 10^5 \text{ pc}^{-3}$, $m = 1 M_\odot$, and a velocity dispersion $\sigma = 10 \text{ km s}^{-1}$. Data from the numerical experiments of [Atallah et al. \(2024, figure 3\)](#) are over-plotted for comparison, and re-scaled according to their equation (20). Details are in the text and appendix C.

formation rate to Γ_v , to the results of previous works: [Goodman & Hut \(1993\)](#) (cf. [Heggie & Hut 2003](#)) obtain, for the equal mass case,

$$\Gamma_{\text{GH}} = 0.75 \frac{G^5 m^5 n^3}{\sigma^9}. \quad (27)$$

We find

$$\lim_{\zeta \rightarrow 0} \Gamma_v = 0.68 \Gamma_{\text{GH}}; \quad (28)$$

that is, the contribution of ergodic hard binary formation to the total rate is roughly 70%, or

$$\Gamma_v = 0.51 \frac{G^5 m^5 n^3}{\sigma^9}. \quad (29)$$

3.3 Orbital Parameter Probabilities

One can play the same exercise, and compute the total formation probability of binaries with given values of the semi-major axis and eccentricity, (a_b, e_b) , given that a binary does form. This is a convex combination of functions of the form (8), with E and J sampled from the distribution of initial conditions described above. That is,

$$\frac{dP}{da_b de} = \frac{1}{P_{\text{bin}}} \left[\frac{m_1 m_2 m_3}{M} \right]^{3/2} \frac{V_0^{-2}}{[2\pi k_B T]^3} \int d^3 r d^3 R d^3 v d^3 V e^{-\frac{E}{k_B T}} f_{\text{bd}}(E_b, S|E, J; R_0) \frac{dE_b}{da_b} \frac{\partial S}{\partial e_b}, \quad (30)$$

where we have made the R_0 dependence of f_{bd} explicit. We evaluate this 6-dimensional integral using Monte Carlo integration. The result is shown in figure 6. Also shown in that figure is the line $e_b = 1 - R_0/a_b$, below which there is zero probability of forming binaries. This effectively forces the soft binaries, with $a_b \geq R_0$, to be very eccentric. To

compare with figure 7 of [Atallah et al. \(2024\)](#) we also plot the cumulative distribution $P(\leq e_b|a_b)$. This is calculated by integrating the probability density in the left panel of figure 6 over eccentricity up to e_b , and normalising, at each value of a_b . The result is shown in the right panel of figure 6. One can see that the two colour maps agree qualitatively, in both $a_b \ll R_0$ and $a_b \gg R_0$ limits, although our $P(\leq e_b|a_b)$ has a ridge which is not present in the simulation results of [Atallah et al. \(2024\)](#); at present, we do not know what gives rise to this ridge.

4 APPLICATION

To summarise, let us describe briefly how to apply the results of this paper to modelling of binary populations in a cluster with a given temperature and density: first, one should calculate ζ with equation (10). Then, compute P_{bin} with equation (C22) and $P_{\text{hard},1,2}$ with equations (C14) and (C18). The rate is then Γ_{3UB} times the probability. For $P_{\text{hard},1}$, if $\zeta \ll 1$ the hard binary formation rate is directly given by (29).

However, one should bear in mind that the orbital parameters a_b and e_b of the binaries that form are highly correlated, and their distribution is also highly dependent on ζ . The conditional probability, $P(e_b|a_b)$ does not appear to depend strongly on ζ from figure 6, and is thus independent of the environment in the astrophysically realistic limit $\zeta \ll 1$. In creating a realistic distribution of three-body binaries one must, therefore, draw them from the joint distribution $P(a_b, e_b)$ in figure 6. For these one has to use equation (8) and the procedure at the end of §3, or equivalently read these off figure 6.

5 DISCUSSION AND SUMMARY

This paper consisted of two main parts: the first is concerned with the three-body problem, giving a probability distribution for the outcome of a three-body scattering experiment, for fixed values of the conserved quantities, i.e. E , \mathbf{J} and the masses. The second part of the paper was an application of the first to a cluster – a system with a certain distribution of conserved quantities (in the equal mass case). This distribution was a Gaussian velocity distribution, while initial positions were assumed to be uniform in a sphere of radius R_0 .

Everything done here assumed some kind of ergodicity or phase-space mixing. The main argument made to support this was that while indeed there are no democratic resonances for an extended period of time, the problem is still chaotic, and whether a binary forms and its final characteristics, do depend very sensitively on the initial conditions because the binding energies required for a binary are much smaller than E . Alternatively, at least for the negative-energy problem, we know that detailed balance arguments produce the same probability distribution as the one obtained from ergodic mixing in the available phase-space volume ([Ginat & Perets 2021a](#)). Here, though, we do not find the same result as [Goodman & Hut \(1993\)](#), which was based on detailed balance, primarily because that work did not account explicitly for angular momentum conservation, but

also because in the negative-energy case, the balance was between bound triples (in a democratic resonance) and binaries and singles, while here there are no democratic resonances.

However, this can also be viewed from the opposite perspective, where the rates that we calculated here are those for three-body binary formation via an ergodic channel. They were slightly lower than those computed from numerical simulations (cf. figure 5), possibly due to non-ergodic three-body binary formation also playing some rôle, or due to inexact matching of the initial condition distribution. But the agreement, albeit imperfect – and the correct scalings with ζ – act as an *a posteriori* validation of the ergodicity assumption.

We found that soft binaries were formed at a much higher rate and that their eccentricity distribution tended to be highly non-thermal (this arose primarily from the restriction $e_b \geq 1 - R_0/a_b$), while hard binaries had a thermal distribution, except at low angular momenta. When $\kappa \approx 0$, the zero angular momentum case for the three-dimensional three-body problem was already known to be very similar to the two-dimensional problem ([Valtonen & Karttunen 2006](#); [Stone & Leigh 2019](#); [Parisichewsky et al. 2021](#); [Samsing et al. 2022](#); [Ginat & Perets 2023](#); [Trani et al. 2024](#); [Fabj & Samsing 2024](#)), which also yields super-thermal eccentricity distributions. That soft binaries are highly preferred (which is corroborated by [Goodman & Hut 1993](#); [Atallah et al. 2024](#)) suggests that these binaries are important in clusters, despite being mostly ignored in the literature,² which is why the findings of this paper are not in disagreement with those of, e.g., [Geller et al. \(2019\)](#), who observed a sub-thermal distribution of binaries in a cluster Monte Carlo simulation but with only hard binaries tracked. Indeed, the minuscule minority of soft binaries that do survive encounters with single stars, and become hard, might not be negligible in comparison with the number of the three-body binaries that form hard at the outset. Moreover, if any gas is present, it is suggested in [Rozner & Perets \(2024\)](#) that dynamical friction from it could counteract the softening effect, and shield some soft binaries from destruction.

That three-body binary formation is a natural mechanism for generating eccentric wide binaries might bear on the recent conundrum of eccentric wide binaries detected in *Gaia* ([Tokovinin 2020](#); [Hamilton 2022](#); [Hwang et al. 2022a,b](#); [Hamilton & Modak 2023](#); [Modak & Hamilton 2023](#)), although those binaries are not globular cluster ones.

One of the key questions raised by [Atallah et al. \(2024\)](#) is the scaling of P_{hard} with ζ (equivalently χ_1). In a typical scattering experiment (e.g. if gravity was a short-distance force), one would expect that the rate of binary formation converges as the maximum impact parameter tends to infinity. This would require $P_{\text{hard}} \sim \zeta^5$, which is what we find if we use the first of equations (25) to calculate the binary formation rate ($P_{\text{hard},1}$ in figure 5). However, [Atallah et al. \(2024\)](#) fit a shallower, $\zeta^{9/2}$ scaling to their results, which incidentally is what we find if we also use the second condition of (25) also for hard binaries ($P_{\text{hard},2}$ in figure 5); this would imply that the total binary formation rate would tend to infinity as $R_0 \rightarrow \infty$. One should observe, though, that it

² See, e.g. [Rozner & Perets \(2023\)](#) for a statistical study of soft binaries in equilibrium.

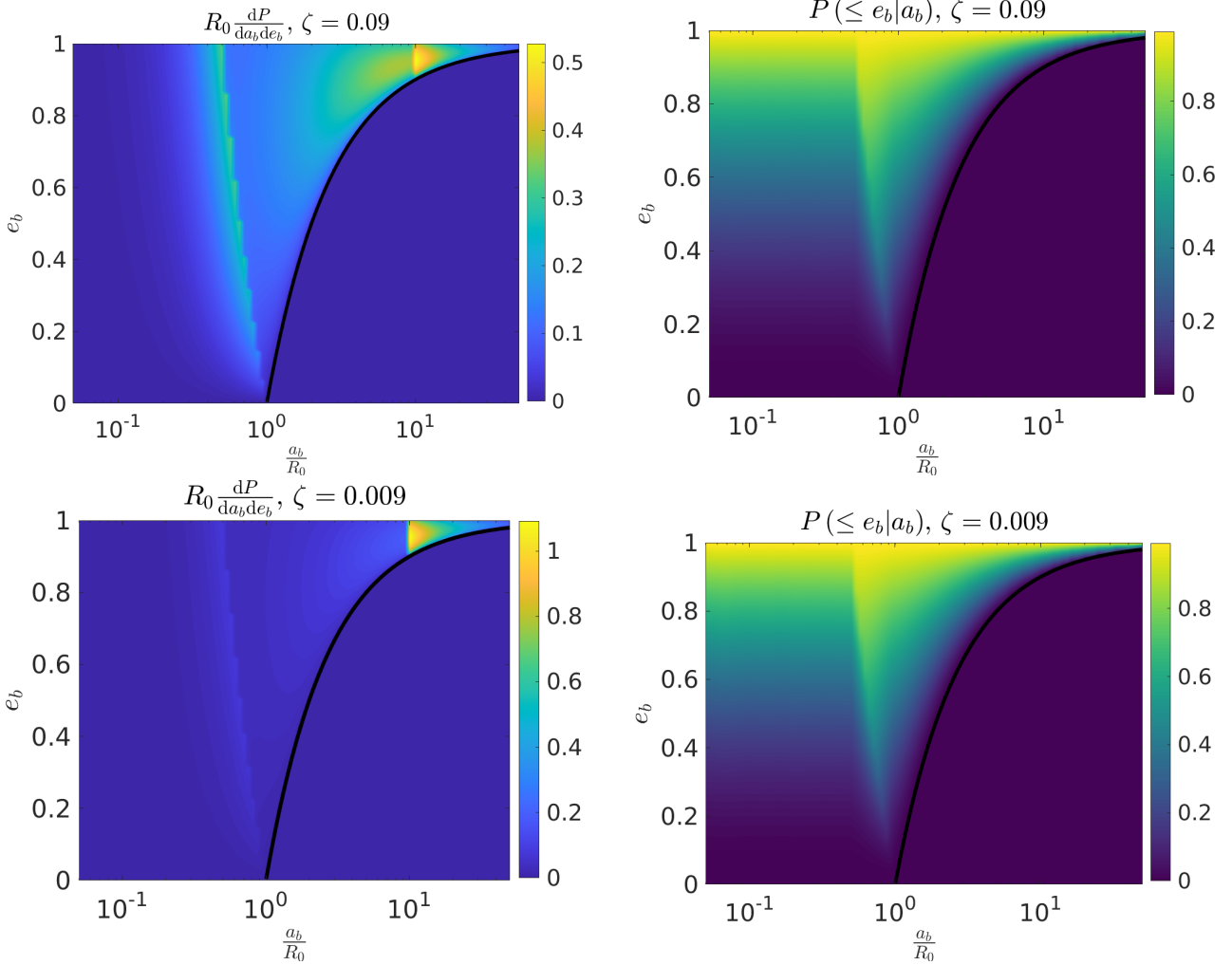


Figure 6. Left: The joint probability distribution of the semi-major axis and the eccentricity of three-body binaries in a cluster. Right: the cumulative eccentricity distribution, given a semi-major axis. These are evaluated for equal masses at $\zeta = 0.09$ (top) and $\zeta = 9 \times 10^{-3}$ (bottom). The black line is $e_b = 1 - R_0/a_b$. While the joint distributions depend on ζ , the conditional eccentricity distribution does not seem to do so, in the $\zeta \ll 1$ limit. See text for more details.

is unclear which of $P_{\text{hard},1}$ and $P_{\text{hard},2}$ follows the scaling of the simulation results better, and that in both cases, the asymptotic scaling is achieved only at very large values of χ_1 , for which there aren't any numerical data. Additionally, ζ (equivalently R_0) is a physical parameter, which is not infinite in real astrophysical systems – it is very small, but finite, determined by the inter-particle separation (or by the Hill radius at the triple's position in the cluster), and the local velocity dispersion there.

ACKNOWLEDGEMENTS

We thank Dany Atallah, Alessandro Trani, and Newlin Weatherford for helpful discussions and for sharing their data, used for figure 5. This work was supported by a Leverhulme Trust International Professorship Grant (No. LIP-2020-014). Y.B.G. was supported in part by the Simons Foundation via a Simons Investigator Award to A.A. Schekochihin. The colour-map for the right panel of figure 6

uses the `Matlab` function `viridis.m` by S. Cobeldick, available [here](#).

DATA AVAILABILITY

No new data were produced for this article. Scripts used to make the figures in this article will be shared upon reasonable request to the corresponding author.

REFERENCES

- Aarseth S. J., 1969, *MNRAS*, **144**, 537
- Aarseth S. J., Heggie D. C., 1976, *A&A*, **53**, 259
- Arca Sedda M., Kamlah A. W. H., Spurzem R., Rizzuto F. P., Naab T., Giersz M., Berczik P., 2023, *MNRAS*, **526**, 429
- Atallah D., Weatherford N. C., Trani A. A., Rasio F., 2024, [arXiv:2402.12429 e-prints](#), p. [arXiv:2402.12429](#)
- Binney J., Tremaine S., 2008, *Galactic Dynamics: Second Edition*. Princeton University Press
- Breen P. G., Heggie D. C., 2012a, *MNRAS*, **420**, 309

Breen P. G., Heggie D. C., 2012b, *MNRAS*, **425**, 2493
 Fabian A. C., Pringle J. E., Rees M. J., 1975, *MNRAS*, **172**, 15
 Fabj G., Samsing J., 2024, *arXiv e-prints*, p. [arXiv:2402.16948](#)
 Floria L., 1995, *AJ*, **110**, 940
 Geller A. M., Leigh N. W. C., Giersz M., Kremer K., Rasio F. A., 2019, *ApJ*, **872**, 165
 Generozov A., Stone N. C., Metzger B. D., Ostriker J. P., 2018, *Monthly Notices of the Royal Astronomical Society*, 478, 4030
 Giersz M., 1998, *MNRAS*, **298**, 1239
 Ginat Y. B., Perets H. B., 2021a, *Physical Review X*, **11**, 031020
 Ginat Y. B., Perets H. B., 2021b, *MNRAS*, **508**, 190
 Ginat Y. B., Perets H. B., 2023, *MNRAS*, **519**, L15
 Goodman J., Hut P., 1989, *Nature*, **339**, 40
 Goodman J., Hut P., 1993, *ApJ*, **403**, 271
 Hamilton C., 2022, *ApJ*, **929**, L29
 Hamilton C., Modak S., 2023, *arXiv e-prints*, p. [arXiv:2311.04352](#)
 Heggie D. C., Hut P., 1993, *ApJS*, **85**, 347
 Heggie D., Hut P., 2003, *The Gravitational Million-Body Problem: A Multidisciplinary Approach to Star Cluster Dynamics*. Cambridge University Press, Cambridge, doi:10.1017/CBO9781139164535
 Hong J., Askar A., Giersz M., Hypki A., Yoon S.-J., 2020, *MNRAS*, **498**, 4287
 Hut P., 1996, in Hut P., Makino J., eds, *International Astronomical Union Symposia Vol. 174, Dynamical Evolution of Star Clusters: Confrontation of Theory and Observations*. p. 121 ([arXiv:astro-ph/9605019](#)), doi:10.48550/arXiv.astro-ph/9605019
 Hwang H.-C., Ting Y.-S., Zakamska N. L., 2022a, *MNRAS*, **512**, 3383
 Hwang H.-C., El-Badry K., Rix H.-W., Hamilton C., Ting Y.-S., Zakamska N. L., 2022b, *ApJ*, **933**, L32
 Ivanova N., Belczynski K., Fregeau J. M., Rasio F. A., 2005, *MNRAS*, **358**, 572
 Kol B., 2021, *Celestial Mechanics and Dynamical Astronomy*, **133**, 17
 Kumamoto J., Fujii M. S., Tanikawa A., 2019, *MNRAS*, **486**, 3942
 Mansbach P., 1970, *ApJ*, **160**, 135
 Modak S., Hamilton C., 2023, *MNRAS*, **524**, 3102
 Monaghan J. J., 1976a, *MNRAS*, **176**, 63
 Monaghan J. J., 1976b, *MNRAS*, **177**, 583
 Morscher M., Pattabiraman B., Rodriguez C., Rasio F. A., Umbreit S., 2015, *ApJ*, **800**, 9
 Parischewsky H. D., Ceballos G., Trani A. A., Leigh N. W. C., 2021, *arXiv e-prints*, p. [arXiv:2108.06335](#)
 Park D., Kim C., Lee H. M., Bae Y.-B., Belczynski K., 2017, *MNRAS*, **469**, 4665
 Pooley D., et al., 2003, *ApJ*, **591**, L131
 Portegies Zwart S. F., McMillan S. L. W., 2000, *ApJ*, **528**, L17
 Press W. H., Teukolsky S. A., 1977, *ApJ*, **213**, 183
 Rodriguez C. L., et al., 2022, *ApJS*, **258**, 22
 Rozner M., Perets H. B., 2023, *ApJ*, **955**, 134
 Rozner M., Perets H. B., 2024, *arXiv e-prints*, p. [arXiv:2404.01384](#)
 Rozner M., Generozov A., Perets H. B., 2023, *MNRAS*, **521**, 866
 Samsing J., et al., 2022, *Nature*, **603**, 237
 Shu F. H., Adams F. C., Lizano S., 1987, *ARA&A*, **25**, 23
 Stodolkiewicz J. S., 1986, *Acta Astron.*, **36**, 19
 Stone N. C., Leigh N. W. C., 2019, *Nature*, **576**, 406
 Sundman K. F., 1913, *Acta Mathematica*, **36**, 105
 Tanikawa A., 2013, *MNRAS*, **435**, 1358
 Tokovinin A., 2020, *MNRAS*, **496**, 987
 Trani A. A., Quaini S., Colpi M., 2024, *A&A*, **683**, A135
 Valtonen M., Karttunen H., 2006, *The Three-Body Problem*. Cambridge University Press, Cambridge
 Wang L., et al., 2016, *MNRAS*, **458**, 1450
 Weatherford N. C., Kiroğlu F., Fragione G., Chatterjee S., Kremer K., Rasio F. A., 2023, *ApJ*, **946**, 104
 van Albada T. S., 1968, *Bull. Astron. Inst. Netherlands*, **20**, 57

APPENDIX A: LIMITS FROM SUNDMAN'S INEQUALITY

Sundman's inequality states that $J^2 \leq 2IK$, with I equal to the triples moment of inertia, $I \equiv \sum_i m_i r_i^2$, and K denoting the total kinetic energy. We approximate $I \approx MR_0^2/3$. If E is of the same order as the cluster's thermal energy, $k_B T$, then for $\zeta \ll 1$, $K \approx E$, and then Sundman's inequality becomes $\kappa \leq \frac{2}{3}(\zeta k_B T/E)^{-2}(M/\mu)^3$. For $\zeta \gg 1$, when the triple has mutual separations R_0 , $K \approx 3GM_2^2/R_0$, whence Sundman's inequality becomes $\kappa \leq 2M_2^2 M/\mu^3 (\zeta k_B T/E)^{-1}$. We join the two cases continuously, i.e. by

$$\kappa \leq \kappa_1 \equiv \frac{2M^3}{\mu^3} \begin{cases} \frac{1}{3} \left(\frac{E}{\zeta k_B T} \right)^2 & \text{if } \frac{\zeta k_B T}{E} \leq \frac{M^2}{3M_2^2}, \\ \frac{M_2^2}{M^2} \frac{E}{\zeta k_B T} & \text{otherwise.} \end{cases} \quad (\text{A1})$$

In the case of unequal masses, another bound can be useful:

$$\kappa \leq \frac{E}{G^2 M^2 \mu^3} (L_{\max}^2 + S_{\max}^2 + 2L_{\max} S_{\max}). \quad (\text{A2})$$

Approximate upper limits for the inner and outer angular momenta are $L_{\max} \lesssim \mu V R_0$ and $S_{\max} \lesssim \mu_b v R_0$, whence

$$\kappa \lesssim \kappa_2 \equiv \frac{2M^2}{\mu^2} \frac{E}{\zeta k_B T} \left(\frac{E_s \mu + E_b \mu_b + 2\sqrt{\mu \mu_b E_s E_b}}{\zeta \mu k_B T} \right). \quad (\text{A3})$$

We define $\kappa_{\max} \equiv \min\{\kappa_1, \kappa_2\}$.

For equal masses this simplifies to

$$\kappa_1 = \frac{243}{4} \begin{cases} \left(\frac{E}{\zeta k_B T} \right)^2 & \text{if } \frac{\zeta k_B T}{E} \leq 3, \\ \frac{1}{3} \frac{E}{\zeta k_B T} & \text{otherwise.} \end{cases} \quad (\text{A4})$$

$$\kappa_2 = \frac{81}{2} \frac{E}{\zeta k_B T} \left[\sqrt{\frac{E_s}{\zeta k_B T}} + \sqrt{\frac{3E_b}{4\zeta k_B T}} \right]^2$$

$$\kappa_{\max} = \min\{\kappa_1, \kappa_2\}.$$

APPENDIX B: SCALING OF THE HARD BINARY FORMATION PROBABILITY WITH PARAMETERS

The two parameters p_{hard} can depend on – in addition to κ – are the ratio $E/(k_B T)$ and the ratio $R_0 E/(GM^2)$ (in the equal mass case). We explained already in §2.4 why

$$p_{\text{hard}} \propto \left[\frac{E}{k_B T} \right]^2 p_0 \left(\kappa \frac{k_B T}{E} \right), \quad (\text{B1})$$

so in this appendix we will argue that if $R_0 E/(GM^2) \gg 1$, $p_{\text{hard}} \propto R_0^{-2}$. This dependence clearly comes from the entire phase-space volume, i.e. the normalisation of f in equation (1). This is readily seen by observing that for hard binaries, the integration boundaries for E_b are such that $R_0/a_b \gg 1$, so $\theta_{\max}(R_0, E_b, S) = 2\pi$ always, and nothing seemingly depends on R_0 . But of course, equation (1) is not normalised, and the normalisation

$$N = \iiint dE_b d^2 S m_b \frac{\theta_{\max}(R_0, E_b, S) \theta_{\max}(R, E_s, |\mathbf{J} - \mathbf{S}|)}{|\mathbf{J} - \mathbf{S}| E_s^{3/2} |E_b|^{3/2}} \quad (\text{B2})$$

does depend on R_0 . Obviously, $N = 0$ when $R_0 = 0$ and $N = \infty$ when $R_0 = \infty$ – where there is no cut-off, because the integral over E_b diverges at $E_b = 0$. In fact, we will show

that $N \propto R_0^2$ (for a fixed κ) in the large R_0 limit, which will prove that $p_{\text{hard}} \propto R_0^{-2}$.

Because N diverges as $R_0 \rightarrow \infty$, it is dominated by the region around $E_b = 0$, and in fact by the unbound side, $E_b > 0$ (as we will show below). We therefore consider

$$N_\varepsilon \equiv \int_0^{\varepsilon E} dE_b \iint d^2S \quad (B3)$$

$$m_b \frac{\theta_{\text{max}}(R_0, E_b, S) \theta_{\text{max}}(R_s, E_s, |\mathbf{J} - \mathbf{S}|)}{|\mathbf{J} - \mathbf{S}| E_s^{3/2} |E_b|^{3/2}}.$$

We choose ε such that

$$\frac{GM^2}{R_0 E} \ll \varepsilon \ll 1, \quad (B4)$$

whence, $N \approx N_\varepsilon$ to leading order. According to [Ginat & Perets \(2021a, appendix A\)](#), the angular momentum integral evaluates to \mathcal{I} , which, in the case $\varepsilon \ll 1$, is $\mathcal{I} \approx J/2$, and θ_{max} becomes θ_{ap} , defined by

$$\theta_{ap} = \sqrt{2 \frac{R_0}{a_b} + \frac{R_0^2}{a_b^2}} - \text{arccosh} \left(1 + \frac{R_0}{a_b} \right). \quad (B5)$$

Therefore

$$N_\varepsilon \approx \frac{m_b J}{2} \int_0^{\varepsilon E} dE_b \frac{\theta_{ap}(R_0, E_b) \theta_{ap}(R_s, E_s)}{E_s^{3/2} |E_b|^{3/2}}. \quad (B6)$$

Again, because $\varepsilon \ll 1$, we have $E_s \approx E$ and $E_b \ll E$, so $\theta_{ap}(R_s, E_s) = \theta_{ap}(R_0, E) \approx 2R_0 E / (GM\mu_s)$ (because for $E_b > 0$, $R_s = R_0$), so

$$N_\varepsilon \approx \frac{2m_b J R_0}{GM\mu_s E^2} \int_0^{\varepsilon E} dE_b \frac{\theta_{ap}(R_0, E_b)}{|E_b|^{3/2}}. \quad (B7)$$

Let us change variables to $x = R_0/a_b = 2R_0 E_b / (Gm_b \mu_b)$, and use the integral

$$\int_0^x \frac{1}{y^{3/2}} \left[\sqrt{2y + y^2} - \text{arccosh}(1 + y) \right] dy$$

$$= \frac{2\sqrt{x(x+2)}}{\sqrt{x}} - 2\sqrt{2} \ln \left[2\sqrt{x} + \sqrt{2}\sqrt{x(x+2)} \right] - 4\sqrt{2}$$

$$+ \sqrt{2} \ln(x) + 2\sqrt{2} \ln \left(\sqrt{2}\sqrt{x+2} + 2 \right) + \frac{2\text{arccosh}(x+1)}{\sqrt{x}}, \quad (B8)$$

which grows like $2\sqrt{x}$ at large x . These yield

$$N_\varepsilon \approx \frac{m_b J R_0}{GM\mu_s E^2} \sqrt{\frac{2R_0}{Gm_b \mu_b}} \int_0^{\frac{2R_0 \varepsilon E}{Gm_b \mu_b}} dx \frac{\theta_{ap}(x)}{x^{3/2}}. \quad (B9)$$

Luckily, $\frac{2R_0 \varepsilon E}{Gm_b \mu_b} \gg 1$ because of our choice of ε , so we can use the asymptotic $\int_0^x \theta_{ap}(x') x'^{-3/2} dx' \sim 2\sqrt{x}$; this gives

$$N_\varepsilon \approx \frac{m_b J R_0}{GM\mu_s E^2} \frac{2R_0 \sqrt{\varepsilon}}{Gm_b \mu_b} = \frac{4J}{G^2 M \mu_s \mu_b} R_0^2 \sqrt{\varepsilon}. \quad (B10)$$

The dependence on ε is immaterial, but importantly N_ε – and therefore N – grows quadratically with R_0 in this limit.

Now consider the marginally bound binaries, contributing to

$$N_{\text{mb}, \varepsilon} \equiv \int_{-\varepsilon E}^0 dE_b \iint d^2S \quad (B11)$$

$$m_b \frac{\theta_{\text{max}}(R_0, E_b, S) \theta_{\text{max}}(R_s, E_s, |\mathbf{J} - \mathbf{S}|)}{|\mathbf{J} - \mathbf{S}| E_s^{3/2} |E_b|^{3/2}}.$$

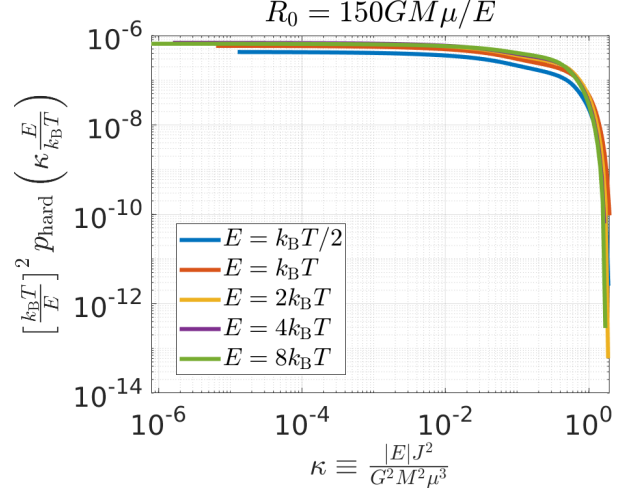


Figure B1. A comparison of the scaling in equation (16) with a direct integration of equation (8) for various values of the hard-soft boundary (i.e. multiples of $k_B T$). The scaling is approximately satisfied by p_{hard} , with only the highest temperature performing worse; we suspect that this discrepancy is due to the extreme smallness of p_{hard} there.

This integral evaluates similarly, except one difference: while $\theta_{ap}(R_s, E_s) \approx 2R_0 E / (GM\mu_s)$ still, $\theta_{\text{max}}(R_0, E_b, S) \in [0, 2\pi]$, because it is the mean anomaly of an elliptic orbit. Consequently, the integral

$$\int_0^x \frac{\theta_{\text{max}}(y)}{y^{3/2}} dy, \quad (B12)$$

where $y = R_0/a_b$, is now no longer dominated by the upper boundary, so it evaluates to something which depends on R_0 weakly, and for $x \gg 1$ it is approximated by

$$\int_0^\infty \frac{\theta_{ap}(y)}{y^{3/2}} dy = \sqrt{2}(4 - \pi) \approx 1.214. \quad (B13)$$

Therefore,

$$N_{\text{mb}, \varepsilon} \propto R_0^{3/2} \quad (B14)$$

in this limit.

Hence, $N \sim N_\varepsilon \propto R_0^2$, and we have the scalings

$$p_{\text{bin}} \sim \frac{N_{\text{mb}, \varepsilon}}{N_\varepsilon} \propto R_0^{-1/2} \quad (B15)$$

$$p_{\text{hard}} \propto R_0^{-2}. \quad (B16)$$

These prove the scalings in equation (15).

Having derived these scaling relations analytically, let us test them by comparing them with direct numerical integration of equation (1) or equation (8), each time for different values of R_0 and $E/(k_B T)$. Figure B1 shows the scaling with temperature, while figure B2 shows the scaling with R_0 . Both agree qualitatively with the analytical scalings.

Before moving on to calculate the rate, the only remaining function we have to compute for the rate is $P_{\text{hard}}(\kappa) \equiv \int_0^\kappa p_0(\kappa'; d_0) d\kappa'$ (see equation (C14) below). We do so for the same value of R_0 as in the top panel of figure 4. The result is shown in figure B3. To simplify calculations, we tabulate this integral and interpolate between its values, whenever it is required in the rate calculation.

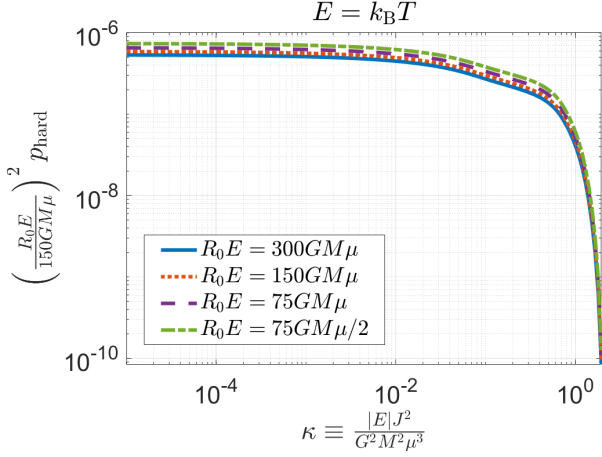


Figure B2. A comparison of the scaling in equation (16) with a direct integration of equation (8) for various values of the cut-off R_0 .

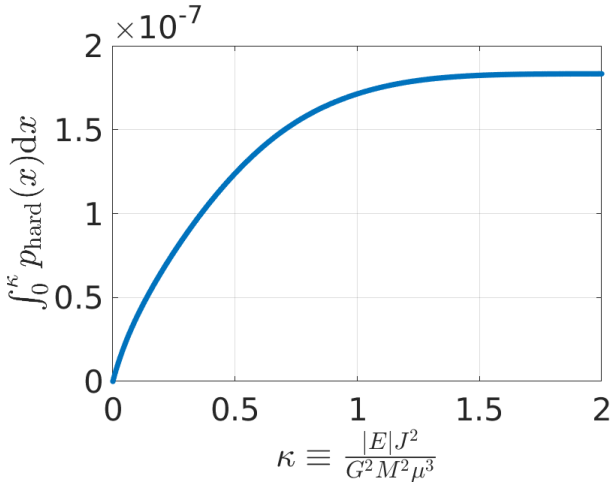


Figure B3. A plot of the integral of p_{hard} over κ , for $R_0 E = 150 GM \mu$. See text for details.

APPENDIX C: RATE CALCULATION

The purpose of this appendix is the calculation of the binary formation probability in equation (22), and likewise the similar calculation for the hard binary formation probability. While doing so, we will derive the scalings (26).

C1 Hard Binaries

Let us start with P_{hard} : we first change variables from \mathbf{r} , \mathbf{v} , \mathbf{R} , \mathbf{V} to hyperbolic Delaunay variables (Floria 1995),³ which are treated here as mere phase-space co-ordinates – we do not claim that the orbit is in fact two hyperbolas, but

³ Here we denote what that paper called l and L by θ_c and J_c . The super-script (or sub-script) i is used to refer to the initial values, and the two other action variables are the absolute value and the $\hat{\mathbf{z}}$ component of the angular momentum.

just use these as a way to sample the initial conditions. The Jacobian is

$$d^3 V d^3 R = \mu_s^{-3} d^3 \theta_s d^3 J_s \quad (\text{C1})$$

$$d^3 v d^3 r = \mu_b^{-3} d^3 \theta_b d^3 J_b. \quad (\text{C2})$$

Moreover, the angle integral is immediately carried out to yield $(2\pi)^4 \times (2\theta_{\text{max}}^b)(2\theta_{\text{max}}^s)$, where θ_{max} incorporates the cut-offs in (25); the factors of 2 come from the possibility of negative mean anomalies, as well as positive ones. We can approximate as above (cf. appendix A of Ginat & Perets 2021a)

$$\theta_{\text{max}} \approx \theta_{ap} \xi(b), \quad (\text{C3})$$

with

$$\theta_{ap}(x) = \sqrt{2x + x^2} - \text{arccosh}(1 + x), \quad (\text{C4})$$

and $b \equiv S/S_{\text{max}}$ [resp. L/L_{max}], while

$$\xi(b) \equiv \sqrt{1 - b^2}(1 + 2b^2), \quad (\text{C5})$$

and $x = R_{\text{max}}/a$, where a is the semi-major axis and R_{max} is the appropriate upper bound on the pericentre distance.

Equation (22), upon replacing P_{bin} with P_{hard} , becomes

$$\begin{aligned} P_{\text{hard}} &= \frac{8\pi\mu_b^{-3}\mu_s^{-3}}{V_0^2} \left(\frac{m_1 m_2 m_3}{M}\right)^{3/2} \frac{1}{(k_B T)^3} \\ &\times \int dJ_{c,s}^i \int dJ_{c,b}^i \int d^2 S_i \int d^2 L_i \xi(b_b) \xi(b_s) \theta_{ap}^b \theta_{ap}^s \\ &\times p_{\text{hard}} e^{-\frac{E}{k_B T}}, \end{aligned} \quad (\text{C6})$$

where J_c^i is the Delaunay action conjugate to the mean anomaly, and \mathbf{S}_i and \mathbf{L}_i are the initial angular momenta. The S_i integral simply evaluates to

$$2\mu_b R_0^2 E_{b,i} \int_0^1 2b\xi(b) db = 3.6\mu_b R_0^2 E_{b,i} \quad (\text{C7})$$

We can now change variables from an integral over \mathbf{L}_i to an integral over the total angular momentum, \mathbf{J} , which goes from 0 to J_{max} , which is nothing but (by definition of κ)

$$J_{\text{max}} = \frac{GM\mu^{3/2}\sqrt{\kappa_{\text{max}}}}{\sqrt{E}}. \quad (\text{C8})$$

Luckily, for equal masses, this, in conjunction with equation (25), implies that b_s is small, whence $\xi(b_s) \approx 1$. Hence,

$$\begin{aligned} P_{\text{hard}} &= \frac{20\pi\mu_b^{-3}\mu_s^{-3}}{V_0^2} \left(\frac{m_1 m_2 m_3}{M}\right)^{3/2} \frac{\mu_b R_0^2}{(k_B T)^3} \\ &\times \int dJ_{c,s}^i \int dJ_{c,b}^i \int_0^{J_{\text{max}}} d^2 J E_b \theta_{ap}^b \theta_{ap}^s p_{\text{hard}} e^{-\frac{E}{k_B T}}. \end{aligned} \quad (\text{C9})$$

We will now change variables from $J_{c,s}^i$ and $J_{c,b}^i$ to the initial energies $E_{s,i}$ and $E_{b,i}$, and from J to κ ; the Jacobians for

this transformation are

$$d\kappa = \frac{2EJ}{G^2M^2\mu_s^3} dJ \quad (\text{C10})$$

$$dJ_{c,s}^i = -\frac{GM\mu_s^{3/2}}{\sqrt{8E_{s,i}^{3/2}}} dE_{s,i} \quad (\text{C11})$$

$$dJ_{c,b}^i = -\frac{Gm_b\mu_b^{3/2}}{\sqrt{8E_{b,i}^{3/2}}} dE_{b,i}. \quad (\text{C12})$$

We will also henceforth drop the i where it isn't confusing to do so. This transforms P_{hard} into

$$P_{\text{hard}} = \frac{5\pi\mu_b R_0^2 G^4 M^3 m_b \mu_s^3}{2V_0^2 (k_B T)^3} \left(\frac{m_1 m_2 m_3}{M\mu_s \mu_b} \right)^{3/2} \times \iint_0^\infty \frac{dE_b dE_s}{(E_b E_s)^{3/2}} \int_0^{\kappa_{\text{max}}} d\kappa \frac{E_b}{E} \theta_{ap}^b \theta_{ap}^s P_{\text{hard}} e^{-\frac{E}{k_B T}}. \quad (\text{C13})$$

Finally, the scaling in equation (16) implies that

$$P_{\text{hard}} = \frac{5\pi\mu_b d_0^2 G^4 M^3 m_b \mu_s^3}{2V_0^2 (k_B T)^4} \left(\frac{m_1 m_2 m_3}{M\mu_s \mu_b} \right)^{3/2} \times \iint_0^\infty \frac{dE_b dE_s}{(E_b E_s)^{3/2}} E_b \theta_{ap}^b \theta_{ap}^s e^{-\frac{E}{k_B T}} \times \int_0^{\kappa_{\text{max}} \frac{k_B T}{E}} du p_0(u; d_0). \quad (\text{C14})$$

Equation (C14) is the equation that we integrate numerically for the plot in figure 5, specifically, the line denoted by $P_{\text{hard},1}$ there. Let us now show that this yields a $\zeta^5 \propto \chi_1^{-5}$ scaling.

C1.1 Scaling at $\zeta \rightarrow 0$

First, note that $V_0^{-2} \propto \zeta^6$. In the limit of small ζ , i.e. large R_0 , the only other dependence on R_0 in equation (C14) can come from $\theta_{ap}^b \theta_{ap}^s$. These are obtained from the constraints in equation (25), which imply that in fact θ_{ap}^s is independent of R_0 , while the argument of θ_{ap}^b , namely

$$\frac{2R_0 E_b}{Gm_b \mu_b} \gg 1 \quad (\text{C15})$$

is very large. Consequently,

$$\theta_{ap}^b \sim \frac{2R_0 E_b}{Gm_b \mu_b} \quad (\text{C16})$$

in this limit (recall that this is the Delaunay angle of a hyperbolic trajectory, which is unbounded). Together, we find

$$P_{\text{hard},1} \sim R_0^{-5} \times \frac{45d_0^2 G^3 M^3 \mu_s^3}{16\pi (k_B T)^4} \left(\frac{m_1 m_2 m_3}{M\mu_s \mu_b} \right)^{3/2} \times \iint_0^\infty \frac{dE_b dE_s}{E_s^{3/2}} E_b^{1/2} \theta_{ap}^s e^{-\frac{E}{k_B T}} \times \int_0^{\kappa_{\text{max}} \frac{k_B T}{E}} du p_0(u; d_0). \quad (\text{C17})$$

Observe, that if we had used the second condition in equation (25), instead of the first, we would have had $\theta_{ap}^s \sim \sqrt{r}$, which is dominated by the large r régime, i.e. $\theta_{ap}^s \sim \sqrt{R_0}$. This extra power of 1/2 would have resulted in an

overall $P_{\text{hard}} \propto R_0^{-9/2}$. This is what is plotted in figure 5 as $P_{\text{hard},2}$, viz.

$$P_{\text{hard},2} = \frac{5\pi\mu_b d_0^2 G^4 M^3 m_b \mu_s^3}{2V_0^2 (k_B T)^4} \left(\frac{m_1 m_2 m_3}{M\mu_s \mu_b} \right)^{3/2} \times \iint_0^\infty \frac{dE_b dE_s}{(E_b E_s)^{3/2}} E_b \theta_{ap}^b \theta_{ap,\text{soft}}^s e^{-\frac{E}{k_B T}} \times \int_0^{\kappa_{\text{max}} \frac{k_B T}{E}} du p_0(u; d_0), \quad (\text{C18})$$

with $\theta_{ap,\text{soft}}^s$ has as its argument

$$\frac{1}{a_b} \frac{2Gm_s \sqrt{\mu_s}}{\sqrt{2E_s}} \cdot \sqrt{\frac{r}{2Gm_b}}. \quad (\text{C19})$$

We also remark that this is the scaling reported by [Atallah et al. \(2024\)](#), but that this scaling would imply that the rate does not converge to a constant at arbitrarily large impact parameters. For this reason, we use $P_{\text{hard},1}$ as P_{hard} in the rest of this paper.

C2 Soft Binaries

We repeat the same procedure as above but only change variables to Delaunay variables in the ‘outer’ orbit, denoted by s . This results in

$$P_{\text{bin}} = \frac{1}{\pi V_0^2 (k_B T)^3} \left(\frac{m_1 m_2 m_3}{M} \right)^{3/2} \times \int d^3 r d^3 v \int dJ_{c,s}^i \theta_{ap}^s \int d^2 L_i p_{\text{bin}} e^{-\frac{E}{k_B T}}. \quad (\text{C20})$$

The integral over \mathbf{L}_i is just $R_{\text{max}}^2 V^2 \mu_s^2$, where

$$R_{\text{max}} \equiv \frac{2Gm_s}{V \sqrt{2Gm_b/r}}. \quad (\text{C21})$$

Additionally, by the arguments in §2.4 and appendix B, p_{bin} scales like $\sqrt{d_0/R_0}$. Besides, the κ dependence is very weak, as the inequality $\kappa \leq \kappa_{\text{max}}$ is satisfied for all energies (for equal masses), if $\zeta < 20.25$; we are concerned with $\zeta \ll 1$, so we just take $p_{\text{bin}}(\kappa) \approx p_{\text{bin}}(\kappa = 0)$.

Repeating the above procedure yields eventually

$$P_{\text{bin}} = \frac{2\sqrt{8}\pi G M \mu_s^{7/2}}{V_0^2 (k_B T)^3} \left(\frac{m_1 m_2 m_3}{M\mu_s^2} \right)^{3/2} \sqrt{\frac{d_0}{R_0}} \bar{p}_{\text{bin}}(d_0) \times \int_0^\infty dv \int_0^{R_0} dr \int_0^\infty dE_s^i \frac{v^2 r^2}{(E_s^i)^{3/2}} \theta_{ap}^s V^2 R_{\text{max}}^2 e^{-\frac{E}{k_B T}}. \quad (\text{C22})$$

This equation is used in figure 5 to give the line denoted by P_{bin} .

Let us now show that it scales like ζ^2 at $\zeta \ll 1$: from (25), $R_{\text{max}}^2 \propto r$, and θ_{ap}^s goes like \sqrt{r} . The integral over r is then proportional to $R_0^{9/2}$. Together with the $R_0^{-13/2}$ already present, this becomes R_0^{-2} . This scaling agrees with that obtained originally by [Aarseth & Heggie \(1976\)](#) analytically and numerically, and more recently in the simulations of [Atallah et al. \(2024\)](#).

This paper has been typeset from a $\text{\TeX}/\text{\LaTeX}$ file prepared by the author.